ABCB1 and ABCG2 Restrict Brain and Testis Accumulation and, Alongside CYP3A, Limit Oral Availability of the Novel TRK Inhibitor Selitrectinib

Wenlong Li[1], Rolf W. Sparidans[2], Margarida L.F. Martins[1], Mujtaba El-Lari[1], Maria C. Lebre[1], Olaf van Tellingen[1], Jos H. Beijnen[1,3,4], and Alfred H. Schinkel[1]

ABSTRACT

Selitrectinib (BAY2731954; LOXO-195) is a promising oral tropomyosin receptor kinase (TRK) inhibitor currently in phase I/II clinical trials for the treatment of histology-agnostic cancers positive for TRK fusions. With therapeutic resistance eventually developing with first-generation TRK inhibitors, selitrectinib was designed to overcome resistance mediated by acquired kinase domain mutations. Using genetically modified mouse models and pharmacological inhibitors, we investigated the roles of the multidrug efflux transporters ABCB1 and ABCG2, and the drug-metabolizing CYP3A enzyme complex in selitrectinib pharmacokinetics. *In vitro*, selitrectinib was markedly transported by mouse Abcg2 and human ABCB1, and modestly by human ABCG2. Following oral administration at 10 mg/kg, selitrectinib brain-to-plasma ratios were increased in *Abcb1a/1b*$^{-/-}$ (twofold) and *Abcb1a/1b;Abcg2*$^{-/-}$ (5.8-fold) compared with wild-type mice, but not in single *Abcg2*$^{-/-}$ mice. Testis distribution showed similar results. mAbcb1a/1b and mAbcg2 each restricted the plasma exposure of selitrectinib: With both systems absent oral availability increased by 1.7-fold. Oral administration of the ABCB1/ABCG2 inhibitor elacridar boosted plasma exposure and brain accumulation in wild-type mice to the same levels as seen in *Abcb1a/1b; Abcg2*$^{-/-}$ mice. In *Cyp3a*$^{-/-}$ mice, plasma exposure of selitrectinib over 4 hours was increased by 1.4-fold and subsequently reduced by 2.3-fold upon transgenic overexpression of human CYP3A4 in liver and intestine. The relative tissue distribution of selitrectinib remained unaltered. Thus, selitrectinib brain accumulation and oral availability are substantially restricted by ABCB1 and ABCG2, and this can be reversed by pharmacological inhibition. Moreover, oral availability of selitrectinib is limited by CYP3A activity. These insights may be useful to optimize the clinical application of selitrectinib.

Background

Neurotrophic tropomyosin receptor kinase (*NTRK*) gene fusions involving *NTRK1, NTRK2*, or *NTRK3* (encoding the neurotrophin receptors TRKA, TRKB, and TRKC, respectively) have been identified in a range of pediatric and adult malignancies as oncogenic drivers (1). These fusions cause ligand-independent constitutive activation of the receptors, triggering signaling pathways involved in cell growth and survival, as well as *in vitro* and *in vivo* transformation of primary cells (2, 3). *NTRK* gene fusions usually occur in a mutually exclusive pattern with other oncogenic drivers in human cancers (2, 4). They therefore represent therapeutically highly actionable drivers of tumor growth (2–5).

Recent studies reveal that patients with *NTRK* fusion-positive cancers treated with first-generation TRK inhibitors, such as entrectinib and larotrectinib, often show high response rates (>75%) and durable responses, independent of tumor histology (6, 7). Unfortunately, acquired therapy resistance, for instance, due to the impaired receptor binding of larotrectinib and other TRK inhibitors resulting from secondary resistance mutations in the TRK solvent front, eventually emerges during treatment, limiting the clinical benefit (8, 9).

Selitrectinib (BAY2731954; LOXO-195, Supplementary Fig. S1A), a next-generation TRK inhibitor, is specially developed through structure modeling to overcome resistance mediated by acquired kinase domain mutations (10, 11). Selitrectinib has shown highly potent and selective activity against all *NTRK* resistance mutations in structure modeling, enzyme assays, cell line assays and studies in animal models (10). Further proof of effectiveness of selitrectinib was obtained in an ongoing phase I trial: A promising response was seen in 45% of patients who had disease progression on a prior TRK inhibitor (12). The safety and expanded efficacy of selitrectinib are currently explored in phase I/II trials involving patients aged ≥1 month with NTRK-rearranged cancers after prior treatment with a kinase inhibitor known to inhibit TRK (NCT03215511; NCT03206931; ref. 11).

Multispecific transmembrane transporters, especially the ATP-binding cassette (ABC) and solute carrier transporters, are of considerable pharmacological significance as for many drugs they affect drug disposition and hence therapeutic efficacy and adverse drug reactions (13). Two main drug efflux transporters, P-glycoprotein (ABCB1; MDR1) and breast cancer resistance protein (ABCG2; BCRP), are highly expressed at critical blood–tissue barrier sites, such as the blood–brain barrier (BBB) and blood–testis barrier, as well as in excretory organs (liver, intestine, and kidney; ref. 14). These transporters are also detected in many multidrug-resistant tumors, where they limit the intracellular accumulation of anticancer drugs (14, 15). In addition, poor BBB penetration due to ABC transporters may reduce drug efficacy against primary and secondary brain tumors

[1]Division of Pharmacology, The Netherlands Cancer Institute, Amsterdam, the Netherlands. [2]Division Pharmacology, Department of Pharmaceutical Sciences, Utrecht University, Faculty of Science, Utrecht, the Netherlands. [3]Division of Pharmacoepidemiology and Clinical Pharmacology, Department of Pharmaceutical Sciences, Utrecht University, Faculty of Science, Utrecht, the Netherlands. [4]Department of Pharmacy and Pharmacology, The Netherlands Cancer Institute, Amsterdam, the Netherlands.

Note: Supplementary data for this article are available at Molecular Cancer Therapeutics Online (http://mct.aacrjournals.org/).

Corresponding Author: Alfred H. Schinkel, Division of Pharmacology, The Netherlands Cancer Institute, Plesmanlaan 121, 1066 CX Amsterdam, the Netherlands. Phone: 31–20–512–2046; Fax: 31–20–512–1792; E-mail: a.schinkel@nki.nl

Mol Cancer Ther 2021;20:1173–82

doi: 10.1158/1535-7163.MCT-20-0705

(e.g., brain metastases, gliomas; refs. 16, 17) that often also include *NTRK* fusion-positive cancers. Whether ABCB1 and ABCG2 can transport selitrectinib is still largely unknown.

Drug-metabolizing enzymes are also important in modulating drug absorption, distribution, and elimination. Many drugs and other xenobiotics are metabolized by the cytochrome P450 enzymes (CYP), among which members of the CYP3A family are of special interest (18). CYP3A enzymes display a broad substrate specificity and high inter- and intra-individual variation in expression and activity in liver and intestine (18, 19). CYP3A can thus strongly affect the therapeutic efficacy and toxicity of drugs due to its marked effects on their plasma exposure and oral availability in patients. On the basis of publicly available sources, it is as yet unclear to what extent CYP3A metabolizes selitrectinib.

Here, using genetically modified mouse models and pharmacological inhibitors, we studied the *in vivo* roles of ABCB1 and ABCG2 in modulating selitrectinib oral availability and tissue distribution. Whether mouse and human CYP3A can affect the plasma exposure of selitrectinib was also investigated.

Materials and Methods

Chemicals

Selitrectinib (LOXO-195; >99.5%) was purchased from ChemieTek. Ko143 was obtained from Tocris Bioscience. Elacridar hydrochloride and zosuquidar were from Sequoia Research Products. Heparin (5,000 $IU \cdot mL^{-1}$) was obtained from Leo Pharma and isoflurane from Pharmachemie. BSA Fraction V was purchased from Roche Diagnostics. Other chemicals used in the selitrectinib assay were described before (20). All other reagents and chemicals were purchased from Sigma-Aldrich.

Cell lines and transport assay

Madin–Darby Canine Kidney (MDCK-II) cells (ECACC 00062107) stably transduced with human (h) ABCB1, hABCG2, or mouse (m) Abcg2 cDNA were generated in our institute between 1995 and 2005. The characteristic growth and drug transport properties, including inhibitor sensitivity, were regularly checked to confirm the proper identity and functionality of these polarized epithelial cells. *Mycoplasma* in these cells routinely tested negative. The passage number was 10 to 15 for the transport experiments.

Transepithelial transport assays were done as described before (21) using 12-well plates with microporous polycarbonate membrane filter inserts (3.0-μm pore size, 12-mm diameter, Transwell 3414, Corning). We seeded the parental MDCK-II cells and their subclones at a density of 2.5×10^5 cells per well and allowed 3 days of growth to form an intact monolayer. The integrity of the monolayer membrane was checked and confirmed before and after the transport phase by measuring the transepithelial electrical resistance.

Selitrectinib, zosuquidar (ABCB1 inhibitor), or Ko143 (ABCG2/Abcg2 inhibitor) were dissolved in DMSO at 5 mmol/L, and subsequently diluted 1,000-fold with DMEM medium containing 10% (v/v) FBS to obtain 5 μmol/L solutions. After preincubation with these inhibitors (when appropriate) in both compartments for 1 hour, the transport phase was initiated ($t = 0$) by replacing the donor compartment medium with fresh DMEM containing 10% FBS, 5 μmol/L selitrectinib and inhibitor(s) if applicable. During the experiment, the cells were kept at 37°C, pH∼7.4, in a 5% (v/v) CO_2 environment. A total of 50-μL aliquots were collected at 1, 2, 4, and 8 hours from the acceptor compartment, and stored at −30°C before LC-MS/MS measurement of selitrectinib. The transport ratio r used to describe the active transport of selitrectinib was calculated by dividing the amount of apically directed drug transport by basolaterally directed drug translocation after 8 hours.

Animals

Mouse housing and handling were according to institutional guidelines complying with Dutch and EU legislation. All experimental animal protocols (WP8942, 9067, 9242), including power calculations, designed under the nationally approved DEC/CCD project AVD301002016595 were evaluated and approved by the institutional animal care and use committee. Animals used for this study were male wild-type, *Abcb1a/1b*$^{-/-}$, *Abcg2*$^{-/-}$, *Abcb1a/1b; Abcg2*$^{-/-}$, *Cyp3a*$^{-/-}$, and Cyp3aXAV mice (22–24), all of a >99% FVB genetic background, between 9 and 16 weeks of age with body weights in the range of 26.8–45.2 g. As far as feasible, mice with similar average ages (and body weights) across the experimental cohorts were used. The animals, receiving a standard diet (Transbreed, SDS Diets, Technilab-BMI) and acidified water *ad libitum*, were maintained in a specific pathogen-free and temperature-controlled environment with a 12-hour light and 12-hour dark cycle. Welfare-related assessments were carried out before, during, and after the experiments, with mice showing discomfort levels higher than mild being humanely sacrificed.

Drug stock and working solution

Selitrectinib was dissolved in DMSO at a concentration of 50 mg/mL and further diluted 50-fold with 10 mmol/L hydrochloric acid solution (pH = 2) to reach a concentration of 1 mg/mL in the oral dosing solution. Final concentrations for 10 mmol/L hydrochloric acid and DMSO were 98% and 2% (v/v), respectively. The stock solution of elacridar hydrochloride at 53 mg/mL was prepared in DMSO to obtain 50 mg elacridar base per mL DMSO. To yield a concentration of 5 mg/mL elacridar in the oral dosing solution, the stock solution was diluted 10-fold with a mixture of polysorbate 80, ethanol and water [20:13:67 (v/v/v)]. Elacridar was orally administered at 50 mg/kg body weight. We prepared all dosing solutions freshly on the day of experiment.

Plasma pharmacokinetics and organ accumulation of selitrectinib in mice

Oral administration of selitrectinib to mice using oral gavage directly into the stomach was adopted in this study since selitrectinib is recommended to be taken orally in patients. Mice were first fasted for 2 to 3 hours to minimize variation in absorption upon oral administration. Then selitrectinib (10 mg/kg body weight; 1 mg/mL dosing solution) was administered by gavage into the stomach, with a blunt-ended needle, at 10 μL/g body weight. For the 4- and 1-hour experiment, tail vein serial blood sampling was performed at 0.125, 0.25, 0.5, 1, and 2 hours or at 3, 7.5, 15, and 30 minutes, respectively, using heparinized capillary tubes. After oral administration (4 hours or 1 hour), 5-mL pipette tips were used to cover the snouts of the mice, and they were deeply anesthetized using an isoflurane evaporator with 2% to 3% isoflurane with 0.2 L/min air and 0.1 L/min oxygen forced flow. Cardiac puncture followed to collect blood in Eppendorf tubes containing heparin as an anticoagulant. After sacrificing the anesthetized mice by cervical dislocation, brain, liver, spleen, kidney, small intestine, and testis were rapidly collected. The small intestinal contents (SICs) were separated from small intestinal tissue (SI), which was rinsed by cold saline to remove any residual feces. The plasma fraction was separated from blood cells by centrifugation at 9,000 × g for 6 minutes at 4°C, and collected and stored at −30°C. Brain, liver, spleen,

kidney, small intestinal tissue, SICs, and testis were homogenized with 1, 3, 1, 2, 3, 2, and 1 mL of 4% (w/v) BSA, respectively. All samples were stored at −30°C until analysis.

Brain accumulation of selitrectinib in combination with oral elacridar

For this study, elacridar (50 mg/kg) or vehicle was orally administered at 10 μL/g body weight to wild-type and *Abcb1a/1b;Abcg2*$^{-/-}$ mice. These were then fasted for around 3 hours before oral administration of selitrectinib (10 mg/kg) as detailed above. After selitrectinib administration, serial tail vein blood samples were collected at 3, 7.5, 15, and 30 minutes, and blood, brain, liver, kidney, small intestine with content (SIWC), and testis were isolated at the 1-hour time point. All samples were processed as described above.

LC-MS/MS analysis

A specific and sensitive liquid chromatography-tandem mass spectrometry method for selitrectinib was developed and validated before (20). This was used to determine the concentrations of selitrectinib in DMEM cell culture medium, plasma samples, and organ homogenates.

Pharmacokinetic calculations and statistical analysis

Noncompartmental methods using the software package of PK solutions 2.0.2 (SUMMIT, Research Service) were adopted to calculate pharmacokinetic parameters of selitrectinib as before (21). The area under the curve (AUC) was calculated using selitrectinib plasma concentrations with the linear trapezoidal rule without extrapolating to infinity. The time of peak plasma concentration (T_{max}) and peak plasma concentration (C_{max}) were assessed from the original data of individual mice. GraphPad Prism7 (GraphPad Software) was used to support statistical testing. Heteroscedastic data were log-transformed before applying statistical analysis. The two-sided unpaired Student *t* test was used when differences between two groups were compared. When multiple groups were compared, one-way ANOVA was used and the Bonferroni *post hoc* correction was applied to accommodate multiple testing. Differences were considered statistically significant when $P < 0.05$. All data are presented as geometric mean ± SD.

Results

In vitro transport of selitrectinib in ABC transporter-overexpressing MDCK-II cells

Polarized monolayers of Madin–Darby Canine Kidney (MDCK-II) parental cells and its derivatives transduced with hABCB1, hABCG2 or mAbcg2 cDNA were used to assess transepithelial drug transport as we previously described (25). In the parental cells, a modest apically directed transport of selitrectinib (5 μmol/L) was observed (r = 1.5, **Fig. 1A**). This was fully inhibited by zosuquidar, an ABCB1 inhibitor (r = 0.97, **Fig. 1B**). These data suggest that the low-level endogenous canine ABCB1 could modestly transport selitrectinib. In cells overexpressing hABCB1, the observed pronounced transport of selitrectinib (r = 7.6, **Fig. 1C**) was extensively inhibited by the addition of zosuquidar (r = 0.99, **Fig. 1D**).

To suppress any contribution of endogenous canine ABCB1, zosuquidar was applied in subsequent experiments with hABCG2- and mAbcg2-overexpressing MDCK-II cells. As shown in **Fig. 1E** and **G**, both hABCG2 and mAbcg2 actively transported selitrectinib, with transport ratios of 1.7 and 15.5, versus 0.97 in parental cells, respectively. Ko143, a specific ABCG2 inhibitor, markedly inhibited the transport activity of hABCG2 and mAbcg2 (**Fig. 1F** and **H**). Therefore, selitrectinib is an efficient transport substrate of hABCB1 and mAbcg2, and a modest substrate of hABCG2 and canine ABCB1. These transport data were obtained with a slightly higher starting drug concentration (5 μmol/L) than obtained during peak plasma concentrations in patients (2.1 μmol/L). As the ABC transporters had a substantial impact on selitrectinib transport *in vitro* at concentrations just above the clinical concentrations, it seems likely that they would potentially also affect selitrectinib transport, and thus pharmacokinetics, in patients.

Both ABCB1 and ABCG2 restrict selitrectinib plasma exposure and tissue distribution

To study the possible impact of mAbcb1a/1b and mAbcg2 on systemic exposure and tissue distribution of selitrectinib, a pilot experiment was performed up to 4 hours using male wild-type and combination *Abcb1a/1b;Abcg2*$^{-/-}$ mice, where 10 mg/kg selitrectinib was orally administered. As shown in Supplementary Fig. S2A and Supplementary Table S1, selitrectinib was absorbed very rapidly, with the time to reach peak concentrations occurring at, or earlier than, 7.5 minutes after oral administration. The peak plasma concentration of selitrectinib in *Abcb1a/1b;Abcg2*$^{-/-}$ mice was significantly higher (1.26-fold) than that in wild-type mice, but the plasma exposure of selitrectinib over 4 hours ($AUC_{0-4\,h}$) was not significantly different due to a markedly shorter elimination half-life in *Abcb1a/1b;Abcg2*$^{-/-}$ mice from 2 hours on (Supplementary Fig. S2B). The plasma AUC obtained in wild-type mice was of the same order as seen in patients treated with selitrectinib, albeit at the high end (9,753 ng·h/mL vs. 4,400 ng·h/mL).

The concentrations of selitrectinib in tissues, including brain, liver, spleen, kidney, small intestinal tissue and testis, were also analyzed at 4 hours after dosing. The brain concentration of selitrectinib was around 1.6-fold higher in *Abcb1a/1b;Abcg2*$^{-/-}$ mice compared with wild-type mice, and the brain-to-plasma ratio was 6.8-fold higher (Supplementary Fig. S3A and S3B; Supplementary Table S1). In wild-type mice, the brain-to-plasma ratios were around 0.021, indicating that selitrectinib has a relatively poor intrinsic capacity to accumulate into normal brain. We observed similar results in the testis accumulation of selitrectinib (Supplementary Fig. S3C and S3D; Supplementary Table S1). In contrast, the relative distribution of selitrectinib in other tested tissues was not substantially altered between the two mouse strains based on the tissue-to-plasma ratios (Supplementary Fig. S4).

The single and combined roles of mAbcb1a/1b and mAbcg2 in oral availability and tissue accumulation of selitrectinib were further investigated in a follow-up experiment using male wild-type, *Abcb1a/1b*$^{-/-}$, *Abcg2*$^{-/-}$, and *Abcb1a/1b;Abcg2*$^{-/-}$ mice. To obtain relatively higher plasma levels that are more relevant for evaluating the function of ABC transporters in overall selitrectinib pharmacokinetics, the experiment was terminated at 1 hour. As shown in **Fig. 2A** and **B** and **Table 1**, the plasma $AUC_{0-1\,h}$ was increased by around 1.3- and 1.5-fold in *Abcb1a/1b*$^{-/-}$ and *Abcg2*$^{-/-}$ mice, respectively, compared with wild-type mice, albeit not significantly. However, *Abcb1a/1b;Abcg2*$^{-/-}$ mice showed a highly significant increase (1.7-fold) in plasma exposure compared with wild-type mice. Together, these data indicate that the oral availability of selitrectinib is substantially restricted by the cooperation of mAbcb1a/1b and mAbcg2, and that absence of only one system results in limited changes in selitrectinib systemic exposure.

The brain concentrations of selitrectinib, 1 hour after oral administration, were not significantly different between single *Abcg2*$^{-/-}$ mice and wild-type mice, but single *Abcb1a/1b*$^{-/-}$ mice showed a threefold,

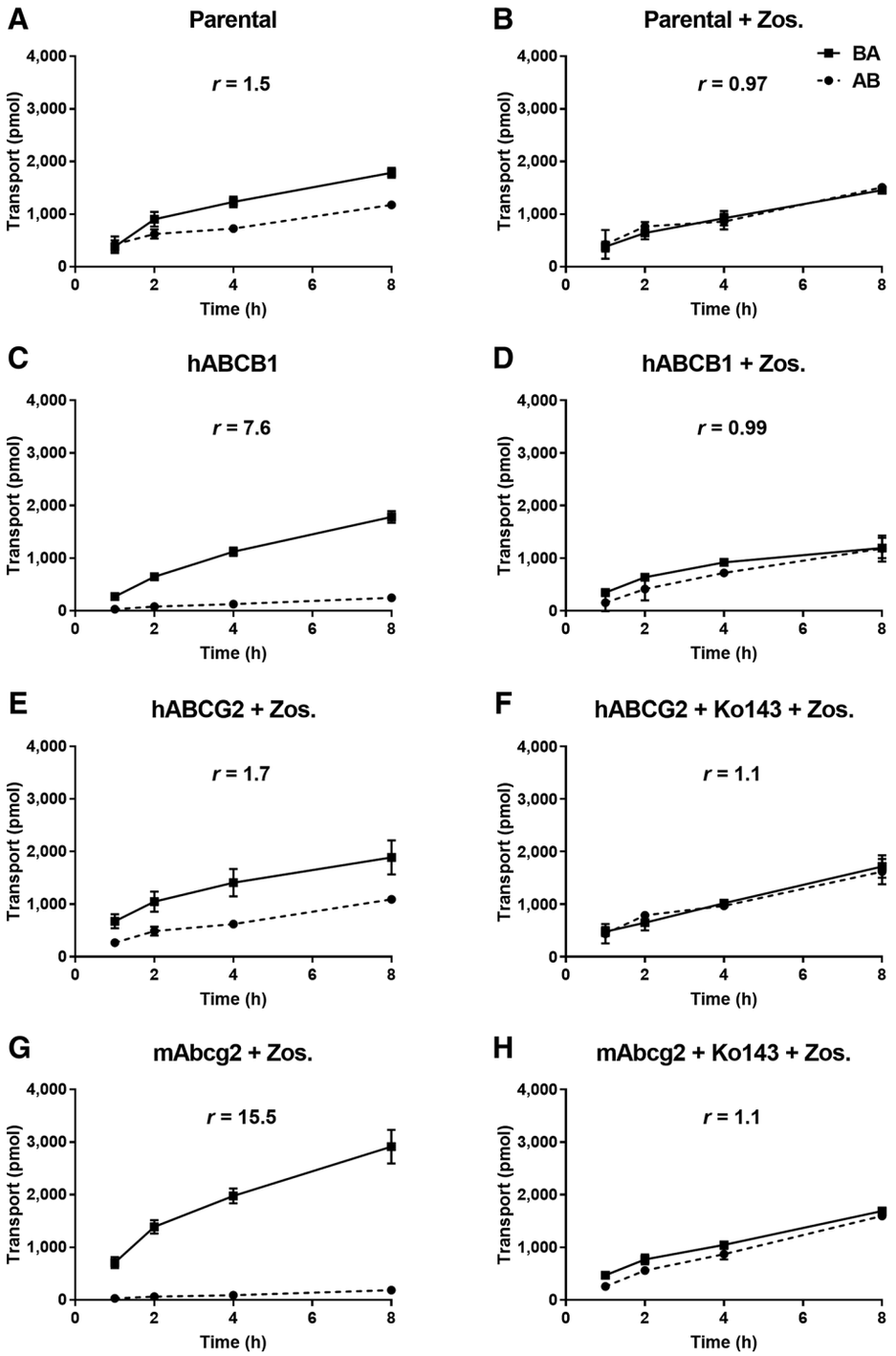

Figure 1.

Transepithelial transport of selitrectinib (5 μmol/L) assessed in MDCK-II cells either non-transduced (**A** and **B**), transduced with hABCB1 (**C** and **D**), hABCG2 (**E** and **F**) or mAbcg2 (**G** and **H**) cDNA. At $t = 0$ hours, selitrectinib was applied in the donor compartment and the concentrations in the acceptor compartment at $t = 1$, 2, 4, and 8 hours were measured and plotted as selitrectinib transport (pmol) in the graph ($n = 3$). **B, D–H**, Zos. (zosuquidar, 5 μmol/L) was applied to inhibit human and/or endogenous canine ABCB1. **F** and **H,** The ABCG2 inhibitor Ko143 (5 μmol/L) was applied to inhibit ABCG2/Abcg2–mediated transport. *r*, relative transport ratio. BA (■, solid line), translocation from the basolateral to the apical compartment; AB (●, dashed line), translocation from the apical to the basolateral compartment. Points, mean; bars, S.D.

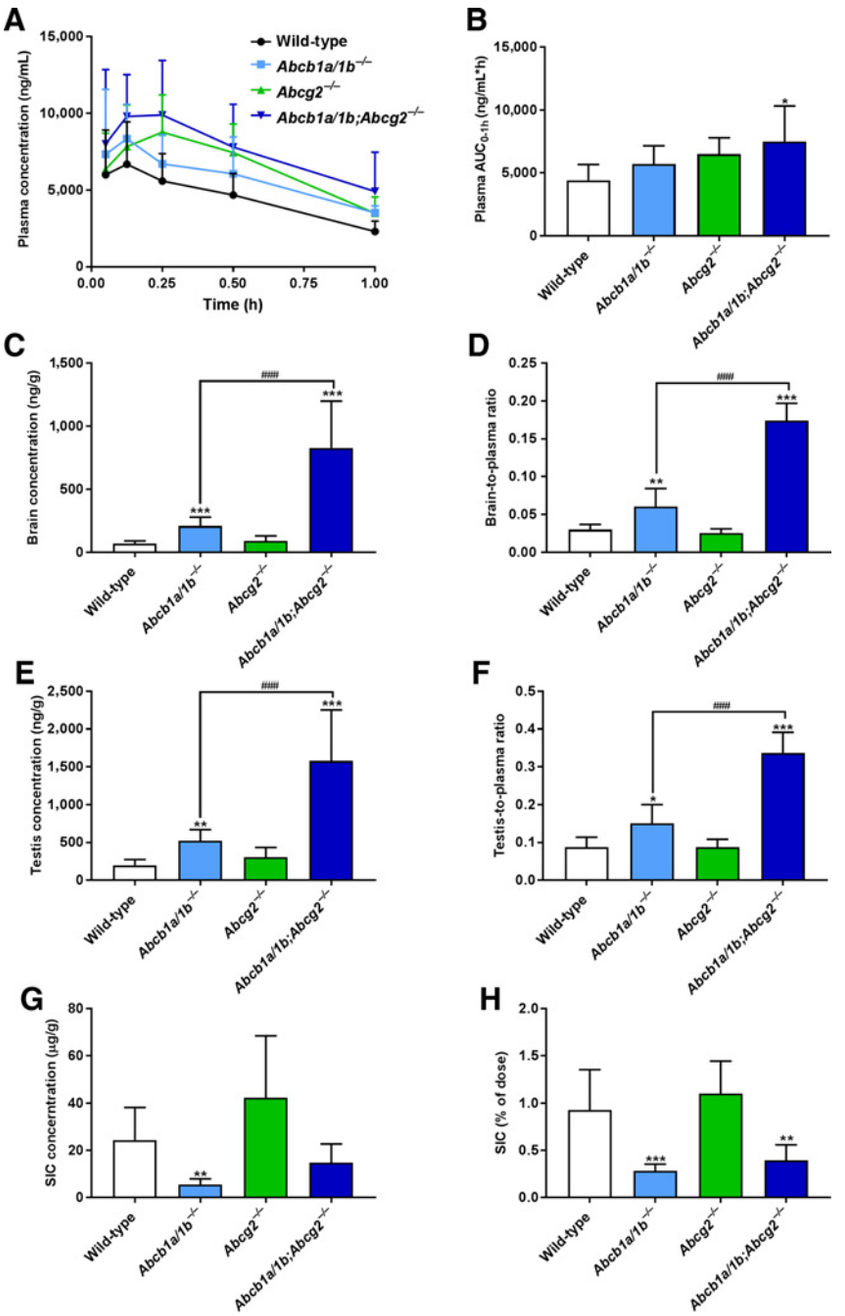

Figure 2.

Plasma concentration–time curves (**A**), plasma $AUC_{0\text{-}1\ h}$ (**B**), brain, testis, small intestinal content (SIC) concentrations (**C**, **E**, and **G**), brain-, testis-to-plasma ratios (**D** and **F**), and SIC as percentage of dose (**H**) of selitrectinib in male wild-type (white bars), *Abcb1a/1b*$^{-/-}$ (light blue bars), *Abcg2*$^{-/-}$ (green bars), and *Abcb1a/1b;Abcg2*$^{-/-}$ (dark blue bars) mice 1 hour after oral administration of 10 mg/kg selitrectinib. Data were first log-transformed before applying statistical analysis. Data are presented as mean ± S.D. ($n = 6$). *, $P < 0.05$; **, $P < 0.01$; ***, $P < 0.001$ compared with wild-type mice. ###, $P < 0.001$ comparing *Abcb1a/1b;Abcg2*$^{-/-}$ mice with *Abcb1a/1b*$^{-/-}$ mice.

and combination *Abcb1a/1b;Abcg2*$^{-/-}$ mice a 12-fold higher brain concentration (**Fig. 2C**; **Table 1**). The intrinsic brain distribution of selitrectinib in wild-type mice was very low, with a brain-to-plasma ratio of 0.03, which substantially rose to 0.06 in *Abcb1a/1b*$^{-/-}$ mice (twofold) and 0.174 in *Abcb1a/1b;Abcg2*$^{-/-}$ mice (5.8-fold), but not in single *Abcg2*$^{-/-}$ mice (**Fig. 2D**; **Table 1**). These data indicate that the brain accumulation of selitrectinib is markedly restricted by mAbcb1, and mAbcg2 can also noticeably participate in this process when mAbcb1 is absent. The testis distribution of selitrectinib behaved qualitatively similar to that in the brain (**Fig. 2E** and **F**; **Table 1**).

Intriguingly, the recovery of selitrectinib (percentage of dose) in the SIC was substantially reduced in the Abcb1a/1b-deficient strains compared with the other mouse strains (**Fig. 2G** and **H**; **Table 1**). This phenomenon could indicate that Abcb1a/1b plays an important role in the enterohepatic circulation of selitrectinib by mediating intestinal excretion, and thus limiting net absorption across the intestinal wall and/or by mediating hepatobiliary excretion in the bile canaliculi of the liver. In other words, the absence of Abcb1a/1b could reduce the intestinal efflux or biliary excretion, or both, leading to a more extensive absorption of selitrectinib. Moreover, in spite of the relatively early time point after selitrectinib oral administration (1 hour), the low amount of selitrectinib recovered in the intestinal lumen (0.3%–1.1% of the dose, **Fig. 2H**) further suggests that selitrectinib was absorbed rapidly and extensively from the intestinal

Table 1. Plasma, brain, testis, liver and small intestine pharmacokinetic parameters of selitrectinib 1 hour after oral administration of 10 mg/kg selitrectinib to male wild-type, *Abcb1a/1b*$^{-/-}$, *Abcg2*$^{-/-}$, and *Abcb1a/1b;Abcg2*$^{-/-}$ mice.

Parameter	Genotype			
	Wild-type	***Abcb1a/1b*$^{-/-}$**	***Abcg2*$^{-/-}$**	***Abcb1a/1b;Abcg2*$^{-/-}$**
$AUC_{0-1\ h}$, ng/mL·h	4,421 ± 1,246	5,706 ± 1,447	6,489 ± 1,304	7,490 ± 2,832*
Fold increase $AUC_{0-1\ h}$	1.00	1.29	1.47	1.69
C_{max}, ng/mL	6,770 ± 2,710	9,210 ± 2,984	10,024 ± 2,174	10,866 ± 3,493
T_{max}, min	7.5–15	≤ 3–15	7.5–30	≤ 3–15
C_{brain}, ng/g	67.9 ± 21.5	208.0 ± 69.6***	89.0 ± 40.9	828.5 ± 370.7***(###)
Fold increase C_{brain}	1.00	3.06	1.31	12.20
Brain-to-plasma ratio	0.030 ± 0.007	0.060 ± 0.024**	0.025 ± 0.006	0.174 ± 0.023***(###)
Fold change ratio	1.00	2.00	0.83	5.80
C_{testis}, ng/g	199 ± 75	523 ± 146**	303 ± 131	1,579 ± 674***(###)
Fold increase C_{testis}	1.00	2.63	1.52	7.93
Testis-to-plasma ratio	0.087 ± 0.027	0.151 ± 0.050*	0.087 ± 0.021	0.337 ± 0.055***(###)
Fold change ratio	1.00	1.74	1.00	3.87
C_{liver}, ng/g	885 ± 215	1,447 ± 398	2,584 ± 1,768	3,519 ± 1914*
Fold increase C_{liver}	1.00	1.64	2.92	3.98
Liver-to-plasma ratio	0.40 ± 0.07	0.41 ± 0.12	0.70 ± 0.27*	0.70 ± 0.18*
Fold increase ratio	1.00	1.02	1.75	1.75
SIC (% of dose)	0.93 ± 0.428	0.29 ± 0.070***	1.10 ± 0.344	0.39 ± 0.165**
Fold change	1.00	0.31	1.18	0.42

Note: Data are presented as mean ± S.D. ($n = 6$). $AUC_{0-1\ h}$, area under the plasma concentration-time curve; C_{max}, maximum concentration in plasma; T_{max}, time point of maximum plasma concentration (range for individual mice); $C_{brain/liver/SIC}$, brain/liver/SIC (small intestinal content) concentration; SIC (% of dose), drug as percentage of dose present in SIC. *, $P < 0.05$; **, $P < 0.01$; ***, $P < 0.001$ compared with wild-type mice. #, $P < 0.05$; ##, $P < 0.01$; ###, $P < 0.001$ comparing *Abcb1a/1b;Abcg2*$^{-/-}$ mice with *Abcb1a/1b*$^{-/-}$ mice.

lumen. Because the selitrectinib concentration in SIC was roughly 10-fold higher than that in small intestinal tissue, this latter compartment likely passively followed the same profile as SIC between the mouse strains.

As shown in Supplementary Fig. S5B and **Table 1**, significantly higher liver-to-plasma ratios were observed in *Abcg2*$^{-/-}$ and *Abcb1a/1b;Abcg2*$^{-/-}$ mice, but not in *Abcb1a/1b*$^{-/-}$ compared with wild-type mice. In contrast, no significant differences were observed in spleen and kidney distribution of selitrectinib among the mouse strains.

Coadministration of elacridar boosts brain and testis distribution of selitrectinib

In view of the limited selitrectinib penetration into wild-type brain due to Abcb1a/1b and Abcg2 activity, we next investigated to what extent we could modulate both efflux systems at the BBB. We used the dual ABCB1/ABCG2 inhibitor elacridar aiming to boost (increase) brain accumulation of selitrectinib, as this principle might potentially benefit treatment of certain brain malignancies. In mice, the peak concentration of elacridar occurs approximately 4 hours after oral administration. This experiment was terminated at 1 hour to optimally assess the plasma and brain selitrectinib levels. Elacridar (50 mg/kg) or vehicle was therefore administered orally 3 hours before oral selitrectinib (at 10 mg/kg) to wild-type and *Abcb1a/1b;Abcg2*$^{-/-}$ mice, aiming to ensure complete inhibition of the ABC transporters in the BBB. In the absence of elacridar, the selitrectinib plasma $AUC_{0-1\ h}$ was significantly (1.6-fold) higher in *Abcb1a/1b;Abcg2*$^{-/-}$ mice compared with wild-type mice, consistent with preceding experiments. Pretreatment with elacridar boosted the plasma $AUC_{0-1\ h}$ of selitrectinib in wild-type mice by 1.6-fold, but no significant change was observed in *Abcb1a/1b;Abcg2*$^{-/-}$ mice (**Fig. 3A** and **B**; **Table 2**).

As shown in **Fig. 3D** and **Table 2**, in vehicle-treated mice, the brain-to-plasma ratios in *Abcb1a/1b;Abcg2*$^{-/-}$ mice were 8.5-fold higher compared with wild-type mice. Unlike the modest impact on plasma exposure, coadministration of elacridar increased the brain concentration and brain-to-plasma ratio of selitrectinib by 11.6- and 8.1-fold ($P < 0.001$) in wild-type mice, respectively, yielding similar levels as those in vehicle-treated *Abcb1a/1b;Abcg2*$^{-/-}$ mice (**Fig. 3C** and **D**; **Table 2**). Interestingly, in the presence of elacridar, brain-to-plasma ratios of selitrectinib further increased significantly by 1.4-fold in *Abcb1a/1b;Abcg2*$^{-/-}$ mice (**Fig. 3D**; **Table 2**). This suggests that elacridar may also inhibit some selitrectinib efflux transport system(s) in the BBB other than Abcb1a/1b and Abcg2, further boosting the brain accumulation of selitrectinib. Pretreatment with elacridar also increased the selitrectinib testis distribution in wild-type, in a pattern very similar to that seen for brain (**Fig. 3E** and **F**). In contrast, the liver and kidney distributions of selitrectinib in both mouse strains were not significantly affected by elacridar treatment (Supplementary Fig. S6).

In the presence of elacridar, the concentration and total amount of selitrectinib present in the SIWC in wild-type mice decreased by around twofold, reaching levels similar to those seen in *Abcb1a/1b;Abcg2*$^{-/-}$ mice with or without elacridar treatment. In accordance with previous results, selitrectinib was absorbed extensively from the intestinal lumen at 1 hour in wild-type mice, with 1.7% of dose recovered in SIWC, which was further markedly reduced to 0.79% upon elacridar coadministration. In contrast, no significant differences were observed in the recovery of selitrectinib (percentage of dose) in the SIWC between elacridar-treated wild-type mice and vehicle- or elacridar-treated *Abcb1a/1b;Abcg2*$^{-/-}$ mice (**Fig. 3G** and **H**; **Table 2**). This suggests that mouse Abcb1a/1b and Abcg2 in the bile canaliculi of the liver and/or small intestine were completely inhibited by elacridar.

CYP3A markedly restricts oral availability of selitrectinib

To investigate the possible impact of mouse Cyp3a and human CYP3A4 on the pharmacokinetics of oral selitrectinib (10 mg/kg), we performed a 4-hour experiment with male wild-type, *Cyp3a*$^{-/-}$

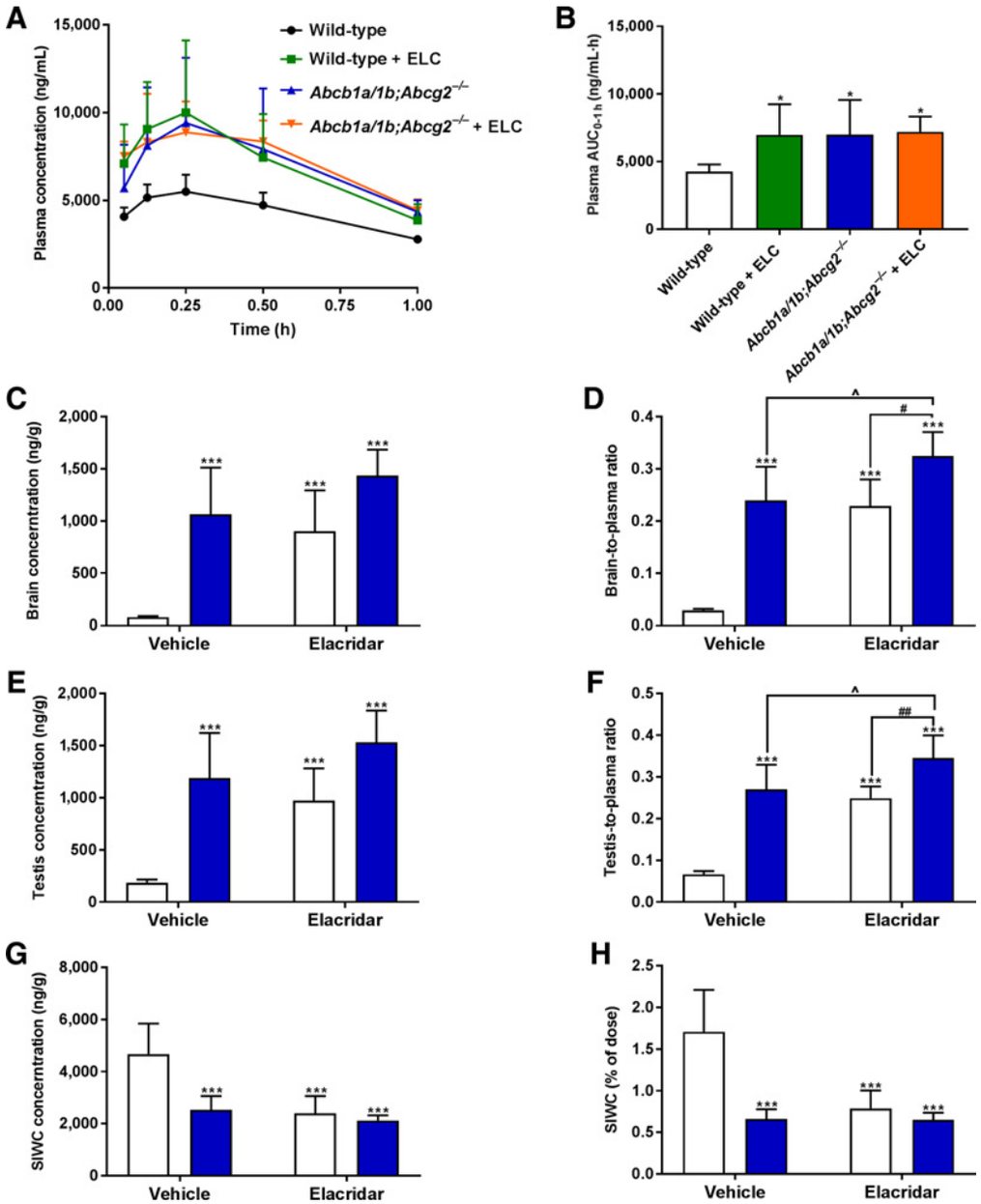

Figure 3.

Plasma concentration–time curves (**A**), plasma $AUC_{0-1\,h}$ (**B**), brain, testis, small intestine with content (SIWC) concentrations (**C**, **E**, and **G**), brain-, testis-to-plasma ratios (**D** and **F**), and SIWC as percentage of dose (**H**) of selitrectinib in male wild-type (white bars) and *Abcb1a/1b;Abcg2*$^{-/-}$ mice (blue bars) 1 hour after oral administration of 10 mg/kg selitrectinib without or with 3 hours preceding oral elacridar (50 mg/kg) coadministration. Data are presented as mean ± S.D. ($n = 6$). *, $P < 0.05$; **, $P < 0.01$; ***, $P < 0.001$ compared with vehicle-treated wild-type mice; $^{\#}$, $P < 0.05$; $^{\#\#}$, $P < 0.01$ comparing elacridar-treated wild-type mice with elacridar-treated *Abcb1a/1b;Abcg2*$^{-/-}$ mice. ^, $P < 0.05$ comparing elacridar-treated with vehicle-treated *Abcb1a/1b;Abcg2*$^{-/-}$ mice.

(Cyp3a knockout), and Cyp3aXAV mice (humanized transgenic mice stably overexpressing CYP3A4 in liver and intestine of *Cyp3a*$^{-/-}$ mice). The absorption of selitrectinib was rapid in all three strains, with T_{max} occurring at or even before 7.5 minutes (**Fig. 4**; Supplementary Table S2). The oral selitrectinib plasma $AUC_{0-4\,h}$ was 1.4-fold higher ($P < 0.001$) in *Cyp3a*$^{-/-}$ mice compared with wild-type mice. In addition, selitrectinib plasma levels in Cyp3aXAV mice were markedly decreased by 1.6-fold and even 2.3-fold relative to wild-type and *Cyp3a*$^{-/-}$ mice, respectively (both $P < 0.001$, **Fig. 4B**). This indicates that mouse Cyp3a and human CYP3A4 play an important role in selitrectinib metabolism and oral availability. Considering the selitrectinib tissue distribution at 4 hours, the observed differences in absolute concentrations in brain, liver, spleen, kidney, small intestinal tissue and testis between the strains mostly reflected the different plasma concentrations, as judged by the effectively unaltered tissue-to-plasma ratios (Supplementary Fig. S7).

Table 2. Plasma, brain, testis, liver and small intestine pharmacokinetic parameters of selitrectinib 1 hour after oral administration of 10 mg/kg selitrectinib to male wild-type and *Abcb1a/1b;Abcg2*$^{-/-}$ mice with vehicle or elacridar coadministration.

Parameter	Genotype and type of pretreatment			
	Vehicle		Elacridar	
	Wild-type	*Abcb1a/1b;Abcg2*$^{-/-}$	Wild-type	*Abcb1a/1b;Abcg2*$^{-/-}$
$AUC_{0-1\ h}$, ng/mL·h	4,267 ± 523	6,988 ± 2,571*	6,980 ± 2,266*	7,205 ± 1,124*
Fold increase $AUC_{0-1\ h}$	1.00	1.64	1.64	1.69
C_{max}, ng/mL	5,601 ± 939	9,425 ± 3,715	10,128 ± 4,023	9,103 ± 1,785
T_{max}, min	7.5–15	15–30	7.5–15	7.5–15
C_{brain}, ng/g	78.1 ± 9.8	1,063 ± 450***	903 ± 390***	1,437 ± 247***
Fold increase C_{brain}	1.00	13.61	11.56	18.40
Brain-to-plasma ratio	0.028 ± 0.003	0.239 ± 0.065***	0.228 ± 0.052***	0.325 ± 0.046***(#)(^)
Fold increase ratio	1.00	8.54	8.14	11.61
C_{testis}, ng/g	184.9 ± 31.3	1,191 ± 431***	973 ± 309***	1,532 ± 306***
Fold increase C_{testis}	1.00	6.44	5.26	8.29
Testis-to-plasma ratio	0.066 ± 0.008	0.270 ± 0.059***	0.249 ± 0.029***	0.346 ± 0.054***(##)(^)
Fold increase ratio	1.00	4.09	3.77	5.24
C_{liver}, ng/g	2,449 ± 335	4,145 ± 1,254	3,765 ± 1,622	4,260 ± 963
Fold increase C_{liver}	1.00	1.69	1.54	1.74
Liver-to-plasma ratio	0.89 ± 0.14	0.95 ± 0.16	0.95 ± 0.16	0.95 ± 0.10
Fold increase ratio	1.00	1.07	1.07	1.07
SIWC (% of dose)	1.71 ± 0.50	0.66 ± 0.12***	0.79 ± 0.21***	0.65 ± 0.08***
Fold change	1.00	0.39	0.46	0.38

Note: Data are presented as mean ± S.D. ($n = 6$). Selitrectinib was administered alone or coadministered with 50 mg/kg oral elacridar 3 hours before selitrectinib administration. $AUC_{0-1\ h}$, area under the plasma concentration-time curve; C_{max}, maximum concentration in plasma; T_{max}, time point of maximum plasma concentration; SIWC, small intestine with content; $C_{brain/testis/SIWC}$, brain/testis/SIWC concentration; SIWC (% of dose), drug as percentage of dose present in SIWC. *, $P < 0.05$; **, $P < 0.01$; ***, $P < 0.001$ compared with vehicle-treated wild-type mice; #, $P < 0.05$; ##, $P < 0.01$ comparing elacridar-treated wild-type mice with elacridar-treated *Abcb1a/1b;Abcg2*$^{-/-}$ mice. ^, $P < 0.05$ comparing elacridar-treated with vehicle-treated *Abcb1a/1b;Abcg2*$^{-/-}$ mice.

Collectively, these results demonstrate that selitrectinib is markedly metabolized by mouse Cyp3a and especially human CYP3A4. This substantially restricts the oral availability, and hence the tissue exposure of selitrectinib.

Discussion

This study shows that the TRK inhibitor selitrectinib is efficiently transported *in vitro* by human ABCB1 and mouse Abcg2 (*r* of 7.6 and 15.5, respectively), and modestly by human ABCG2 and canine ABCB1 (*r* of 1.7 and 1.5, respectively). Although *in vivo* single Abcb1a/1b and Abcg2 deficiency in mice had no significant impact on selitrectinib oral availability, the combined deficiency caused a 1.7-fold increase in plasma $AUC_{0-1\ h}$. Moreover, selitrectinib brain-to-plasma ratios were markedly increased in *Abcb1a/1b*$^{-/-}$ (twofold) and *Abcb1a/1b;Abcg2*$^{-/-}$ (5.8-fold) mice, but not in single *Abcg2*$^{-/-}$ mice, compared with wild-type mice. These transporters in the BBB thus keep selitrectinib out of the brain, with Abcb1a/1b playing the major role. Similar results were obtained for selitrectinib accumulation in the testis. We further observed a clearly reduced concentration and total amount of selitrectinib in the SIC in the absence of Abcb1a/1b. This suggests that ABCB1 can perform direct efflux of selitrectinib from blood across the intestinal wall or its hepatobiliary excretion, or a combination of both functions. On the other hand, ABC transporter deficiency had no noticeable effect on selitrectinib distribution to other tissues. Coadministration of elacridar, a dual ABCB1 and ABCG2 inhibitor, fully reversed the impact of Abcb1a/1b and Abcg2 on brain accumulation and intestinal disposition of selitrectinib. We also found that the oral availability of selitrectinib was substantially restricted by mouse Cyp3a and human CYP3A4. This indicates that CYP3A can likely play an important role in selitrectinib metabolic clearance.

Using structural modeling, selitrectinib was developed as a unique macrocyclic TRK inhibitor, which possesses significantly increased inhibitory activity against all *NTRK*-resistance mutations relative to the first-generation TRK inhibitor larotrectinib (Supplementary Fig. S1B; ref. 7). Moreover, selitrectinib showed better pharmacological properties than larotrectinib (26). Unexpectedly, our data show that brain-to-plasma ratios of selitrectinib were lower than those of larotrectinib. However, at the same dose (10 mg/kg), the peak plasma concentrations and exposure ($AUC_{0-1\ h}$) of selitrectinib in mice were around 13.7- and 11.6-fold higher than those of larotrectinib, still driving markedly higher absolute concentrations and distributions of selitrectinib in brain (26). Importantly, considering the lower nanomolar inhibitory activity achieved by selitrectinib against wild-type and especially mutated TRK compared with larotrectinib, this suggests that selitrectinib may show greater efficacy against brain malignancies driven by TRK fusions.

Compared with lorlatinib (Supplementary Fig. S1C), a macrocyclic ALK/ROS1 inhibitor, a similar compact macrocyclic structure does not appear to endow selitrectinib with an equally high intrinsic BBB permeability: The brain-to-plasma ratios of lorlatinib in wild-type mice are around 0.5 to 0.6, which is around 20-fold higher than what we observed for selitrectinib (27). This indicates that BBB permeability could be affected by several different factors, including, in addition to passive diffusion, uptake and efflux transporters. It is clearly still very challenging to predict the intrinsic BBB permeability of compounds based only on their structure and physicochemical properties.

Similar to larotrectinib and many other TKIs (26, 28), selitrectinib is a transport substrate of both Abcb1a/1b and Abcg2, and *in vivo* subject to collaborative action of these proteins in the BBB. We observed efficient transport of selitrectinib in MDCK-II cells overexpressing mouse Abcg2, with efflux ratios of 15.5 (**Fig. 1G**). However, no

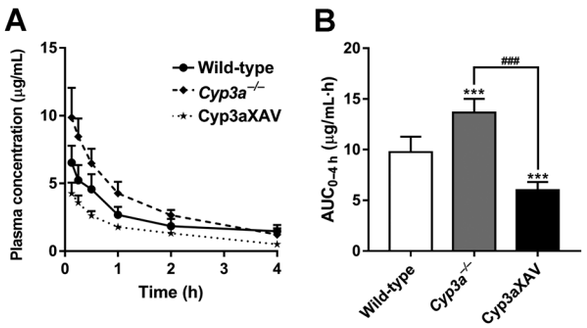

Figure 4.

Plasma concentration–time curves (**A**) and plasma $AUC_{0-4\,h}$ (**B**) of selitrectinib in male wild-type (white bar), *Cyp3a*$^{-/-}$ (gray bar), and Cyp3aXAV (black bar) mice 4 hours after oral administration of 10 mg/kg selitrectinib. Data are given as mean ± S.D. ($n = 6$–7). *, $P < 0.05$; **, $P < 0.01$; ***, $P < 0.001$ compared with wild-type mice. $^{\#}$, $P < 0.01$; $^{\#\#}$, $P < 0.01$; $^{\#\#\#}$, $P < 0.001$ comparing Cyp3aXAV with *Cyp3a*$^{-/-}$ mice.

significant differences were observed in single *Abcg2*$^{-/-}$ mice either in oral availability or brain accumulation, compared with wild-type mice (**Fig. 2**; **Table 1**). The roles of Abcg2 in restricting the brain distribution of selitrectinib became noticeable only in the absence of Abcb1a/1b. These seemingly inconsistent observations from *in vitro* and *in vivo* experiments about the roles of mouse Abcg2 might be related to the higher expression levels of mouse Abcg2 in MDCK-II cells. On the other hand, the expression level of Abcb1a protein is approximately three- to fourfold higher compared with that of Abcg2 at the mouse BBB, which may further weaken the functional impact of BBB Abcg2 in mice (21).

The clear impact of Abcb1a/1b but not Abcg2 on SIC levels of selitrectinib (**Fig. 2H**) contrasts with the impact of Abcg2 but not Abcb1a/1b on the liver concentration and liver-to-plasma ratio of selitrectinib (Supplementary Fig. S5A and S5B). Although speculative, it could be that small intestinal Abcb1a/1b has a stronger impact on the net intestinal absorption of selitrectinib than Abcg2 (**Fig. 2H**), whereas the hepatic Abcg2 could have a stronger impact on biliary excretion than Abcb1a/1b (Supplementary Fig. S5B). In the latter case (*Abcg2*$^{-/-}$), the assumption is that reduced biliary excretion has resulted in a more marked increase in hepatocyte concentrations of selitrectinib, more than offsetting the reduced intrahepatic biliary contribution of the drug. Each of these processes (enhanced intestinal uptake and reduced hepatobiliary excretion) could account for the modestly enhanced oral availability of selitrectinib in each of the single knockout strains, and the additive effect observed in the combination *Abcb1a/1b;Abcg2*$^{-/-}$ knockout strain (**Fig. 2B**). Perhaps counterintuitively, we observed a shorter apparent plasma elimination half-life of selitrectinib in *Abcb1a/1b;Abcg2*$^{-/-}$ compared with wild-type mice, more or less from 1 hour after administration on (Supplementary Fig. S2). We hypothesize that this is the consequence of the longer-lasting and larger dynamic depot of selitrectinib in the intestinal content of wild-type mice, due to the processes described above (**Fig. 2G** and **H**). Ongoing intestinal absorption from this larger depot between 1 and 4 hours after administration, during the plasma elimination phase, results in higher plasma levels of selitrectinib in wild-type mice than in *Abcb1a/1b;Abcg2*$^{-/-}$ mice, and thus an apparently longer half-life.

Given the very limited brain penetration of selitrectinib in wild-type mice owing to ABC transporter functions, and the potential therapeutic benefit of enhancing selitrectinib accumulation in brain malignancies or directly in tumor cells, we tested a potentially clinically realistic schedule to completely inhibit both Abcb1a/1b and Abcg2 in the BBB using coadministration of the pharmacological inhibitor elacridar. Pretreatment with elacridar profoundly increased oral availability and brain accumulation of selitrectinib in wild-type mice, to similar levels as seen in *Abcb1a/1b;Abcg2*$^{-/-}$ mice. This suggests that the activity of Abcb1a/1b and Abcg2 in the BBB, liver, and intestine was completely abrogated by elacridar at this dose. Moreover, brain distribution of selitrectinib in *Abcb1a/1b;Abcg2*$^{-/-}$ mice was further increased by 1.4-fold in the presence of elacridar, suggesting that some other selitrectinib efflux (or perhaps influx) system was affected by elacridar. However, this function could only be noticed when both Abcb1a/1b and Abcg2 were absent.

Of note, some TKI drugs such as the ALK/EGFR inhibitor brigatinib could cause severe and acute CNS toxicity due to ablation or pharmacological inhibition of ABCB1 and ABCG2 in the BBB (28). In contrast, no spontaneous CNS toxicity was observed in any *Abcb1a/1b;Abcg2*$^{-/-}$ mice or elacridar-treated wild-type mice with selitrectinib treatment. Pending further preclinical and clinical evaluation, our findings on elacridar efficacy could therefore provide a rationale for enhanced treatment of primary and secondary brain tumors of *NTRK* fusion-positive cancers by boosting brain penetration of selitrectinib using coadministration of an efficacious ABCB1/ABCG2 inhibitor.

To date, publicly available information on the interaction of selitrectinib with CYP3A is limited. Our *in vivo* results indicate that oral availability and thus overall body exposure of selitrectinib are markedly, but not dramatically, limited by both mouse Cyp3a and human CYP3A4, whereas the relative tissue distribution of the drug remained unaltered. The highly variable CYP3A activity in patients, due to drug–drug and drug–food interactions, genetic polymorphisms, and possibly also some endogenous tumor expression levels, will likely influence the metabolic clearance and systemic exposure of selitrectinib, thus affecting its therapeutic efficacy and even toxicity. Considering future broader use of this drug, this risk will probably need to be weighed in the clinical dosing of selitrectinib. This could mean that coadministration of strong CYP3A-inhibiting or -inducing drugs with selitrectinib should be critically monitored or avoided altogether. Albeit indirectly, the recommendations with clinical phase I/II trials of selitrectinib to exclude "Concurrent treatment with a strong CYP3A4 inhibitor or inducer" (ClinicalTrials.gov) indicate that also the company developing selitrectinib is aware of an interaction risk with CYP3A.

We have demonstrated that *in vitro* selitrectinib is substantially transported by both ABCB1 and ABCG2 and that in mice its oral availability and especially brain distribution are strongly restricted by both ABCB1 and ABCG2. Furthermore, elacridar coadministration could markedly enhance the brain accumulation of oral selitrectinib. Last but not least, mouse Cyp3a and human CYP3A4 can substantially restrict the oral availability of selitrectinib, without altering its relative tissue distribution. The insights and principles obtained from this study may be used to further improve the therapeutic application and efficacy of selitrectinib, especially against brain malignancies.

Authors' Disclosures

J.H. Beijnen reports personal fees from Modra Pharmaceuticals outside the submitted work as well as a patent for oral taxane formulations licensed to Modra Pharmaceuticals. A.H. Schinkel reports other support from Taconic outside the submitted work.

Authors' Contributions

W. Li: Data curation, formal analysis, funding acquisition, validation, investigation, methodology, writing–original draft. **R.W. Sparidans:** Data curation, supervision, validation, investigation, writing–review and editing. **M.L.F. Martins:** Investigation, methodology, writing–review and editing. **M. El-Lari:** Investigation, methodology, writing–review and editing. **M.C. Lebre:** Resources, writing–review and editing. **O. van Tellingen:** Methodology, writing–review and editing. **J.H. Beijnen:** Conceptualization, supervision, project administration, writing–review and editing. **A.H. Schinkel:** Conceptualization, data curation, supervision, writing–original draft, project administration, writing–review and editing.

Acknowledgments

This work was funded in part by the China Scholarship Council (CSC Scholarship No. 201606220081).

The costs of publication of this article were defrayed in part by the payment of page charges. This article must therefore be hereby marked *advertisement* in accordance with 18 U.S.C. Section 1734 solely to indicate this fact.

Received August 17, 2020; revised November 7, 2020; accepted March 12, 2021; published first March 30, 2021.

References

1. Vaishnavi A, Le AT, Doebele RC. TRKing down an old oncogene in a new era of targeted therapy. Cancer Discov 2015;5:25–34.
2. Vaishnavi A, Capelletti M, Le AT, Kako S, Butaney M, Ercan D, et al. Oncogenic and drug-sensitive NTRK1 rearrangements in lung cancer. Nat Med 2013;19:1469–72.
3. Pulciani S, Santos E, Lauver AV, Long LK, Aaronson SA, Barbacid M. Oncogenes in solid human tumours. Nature 1982;300:539–42.
4. Tognon C, Garnett M, Kenward E, Kay R, Morrison K, Sorensen PH. The chimeric protein tyrosine kinase ETV6-NTRK3 requires both Ras-Erk1/2 and PI3-kinase-Akt signaling for fibroblast transformation. Cancer Res 2001;61:8909–16.
5. N TCGAR. Integrated genomic characterization of papillary thyroid carcinoma. Cell 2014;159:676–90.
6. Drilon A, Laetsch TW, Kummar S, DuBois SG, Lassen UN, Demetri GD, et al. Efficacy of larotrectinib in TRK fusion-positive cancers in adults and children. N Engl J Med 2018;378:731–9.
7. Drilon A, Siena S, Ou SI, Patel M, Ahn MJ, Lee J, et al. Safety and antitumor activity of the multitargeted pan-TRK, ROS1, and ALK inhibitor entrectinib: combined results from two phase I trials (ALKA-372–001 and STARTRK-1). Cancer Discov 2017;7:400–9.
8. Russo M, Misale S, Wei G, Siravegna G, Crisafulli G, Lazzari L, et al. Acquired resistance to the TRK inhibitor entrectinib in colorectal cancer. Cancer Discov 2016;6:36–44.
9. O'Reilly EM, Hechtman JF. Tumour response to TRK inhibition in a patient with pancreatic adenocarcinoma harbouring an NTRK gene fusion. Ann Oncol 2019;30:viii36–40.
10. Drilon A, Nagasubramanian R, Blake JF, Ku N, Tuch BB, Ebata K, et al. A next-generation TRK kinase inhibitor overcomes acquired resistance to prior TRK kinase inhibition in patients with TRK fusion–positive solid tumors. Cancer Discov 2017;7:963–72.
11. Cocco E, Scaltriti M, Drilon A. NTRK fusion-positive cancers and TRK inhibitor therapy. Nat Rev Clin Oncol 2018;15:731–47.
12. Combating Acquired TRK Inhibitor Resistance. Cancer discovery.2019;9:684–5.
13. Giacomini KM, Huang SM, Tweedie DJ, Benet LZ, Brouwer KL, Chu X, et al. Membrane transporters in drug development. Nat Rev Drug Discovery 2010;9:215–36.
14. Borst P, Elferink RO. Mammalian ABC transporters in health and disease. Annu Rev Biochem 2002;71:537–92.
15. Schinkel AH, Jonker JW. Mammalian drug efflux transporters of the ATP-binding cassette (ABC) family: an overview. Adv Drug Deliv Rev 2003;55:3–29.
16. Tang SC, Nguyen LN, Sparidans RW, Wagenaar E, Beijnen JH, Schinkel AH. Increased oral availability and brain accumulation of the ALK inhibitor crizotinib by coadministration of the P-glycoprotein (ABCB1) and breast cancer resistance protein (ABCG2) inhibitor elacridar. Int J Cancer 2014;134:1484–94.
17. de Gooijer MC, Zhang P, Weijer R, Buil LCM, Beijnen JH, van Tellingen O. The impact of P-glycoprotein and breast cancer resistance protein on the brain pharmacokinetics and pharmacodynamics of a panel of MEK inhibitors. Int J Cancer 2018;142:381–91.
18. Paine MF, Hart HL, Ludington SS, Haining RL, Rettie AE, Zeldin DC. The human intestinal cytochrome P450 "pie." Drug Metab Dispos 2006;34:880–6.
19. Thelen K, Dressman JB. Cytochrome P450-mediated metabolism in the human gut wall. J Pharm Pharmacol 2009;61:541–58.
20. Sparidans RW, Li W, Schinkel AH, Beijnen JH. Bioanalytical assay for the novel TRK inhibitor selitrectinib in mouse plasma and tissue homogenates using liquid chromatography-tandem mass spectrometry. J Chromatogr B Analyt Technol Biomed Life Sci 2019;1122–1123:78–82.
21. Li W, Sparidans RW, El-Lari M, Wang Y, Lebre MC, Beijnen JH, et al. P-glycoprotein (ABCB1/MDR1) limits brain accumulation and Cytochrome P450–3A (CYP3A) restricts oral availability of the novel FGFR4 inhibitor fisogatinib (BLU-554). Int J Pharm 2020;573:118842.
22. Schinkel AH, Smit JJ, van Tellingen O, Beijnen JH, Wagenaar E, van Deemter L, et al. Disruption of the mouse mdr1a P-glycoprotein gene leads to a deficiency in the blood–brain barrier and to increased sensitivity to drugs. Cell 1994;77:491–502.
23. Jonker JW, Buitelaar M, Wagenaar E, Van Der Valk MA, Scheffer GL, Scheper RJ, et al. The breast cancer resistance protein protects against a major chlorophyll-derived dietary phototoxin and protoporphyria. PNAS 2002;99:15649–54.
24. van Herwaarden AE, Wagenaar E, van der Kruijssen CM, van Waterschoot RA, Smit JW, Song JY, et al. Knockout of cytochrome P450 3A yields new mouse models for understanding xenobiotic metabolism. J Clin Invest 2007;117:3583–92.
25. Li W, Tibben M., Wang Y, Lebre MC, Rosing H, Beijnen JH, et al. P-glycoprotein (MDR1/ABCB1) controls brain accumulation and intestinal disposition of the novel TGF-beta signaling pathway inhibitor galunisertib. Int J Cancer 2020;146:1631–42.
26. Wang Y, Sparidans RW, Li W, Lebre MC, Beijnen JH, Schinkel AH. OATP1A/1B, CYP3A, ABCB1, and ABCG2 limit oral availability of NTRK inhibitor larotrectinib, while ABCB1 and ABCG2 also restrict its brain accumulation. Br J Pharmacol 2020;177:3060–74.
27. Li W, Sparidans RW, Wang Y, Lebre MC, Wagenaar E, Beijnen JH, et al. P-glycoprotein (MDR1/ABCB1) restricts brain accumulation and cytochrome P450–3A (CYP3A) limits oral availability of the novel ALK/ROS1 inhibitor lorlatinib. Int J Cancer 2018;143:2029–38.
28. Li W, Sparidans RW, Wang Y, Lebre MC, Beijnen JH, Schinkel AH. P-glycoprotein and breast cancer resistance protein restrict brigatinib brain accumulation and toxicity, and, alongside CYP3A, limit its oral availability. Pharmacol Res 2018;137:47–55.